Halogenotrimethylplatinum(IV) Complexes of 2,6-Bis(*p*-tolylthiomethyl)pyridine (L^1): Nuclear Magnetic Resonance Studies of their Solution State Stereodynamics and the Crystal Structure of *fac*-[$PtBrMe_3L^1$] †

Edward W. Abel,[a] Peter J. Heard,[a] Keith G. Orrell,*[,a] Michael B. Hursthouse[b] and Mohammed A. Mazid[b]

[a] *Department of Chemistry, The University, Exeter EX4 4QD, UK*

[b] *School of Chemistry and Applied Chemistry, University of Wales, College of Cardiff, Cardiff CF1 3TB, UK*

Under mild conditions 2,6-bis(*p*-tolylthiomethyl)pyridine (L^1) reacted with halogenotrimethylplatinum(IV) to afford complexes of the type *fac*-[$PtXMe_3L^1$] (X = Cl or Br). This potentially terdentate ligand acts here in a five-membered S/N chelate bidentate fashion. Solution dynamic NMR studies revealed the presence of three fluxional processes: pyramidal inversion of the co-ordinated sulfur atom, S–S switching with correlated pyramidal inversion, and S–S switching. The mechanism for the S–S exchange process was elucidated by two-dimensional NMR exchange spectroscopy. The crystal structure of *fac*-[$PtBrMe_3L^1$] confirms the bidentate chelate nature of the ligand in the solid state, with a N–Pt–S(1) angle of 81.5°. IR data for the Pt–C, Pt–N and Pt–X stretching modes in these complexes are also presented.

Metal complexes of ligands with redundant donor atoms are now recognised as potential fluxional species. Suitable donors are Group 15 atoms such as nitrogen and phosphorus, and Group 16 atoms such as sulfur, selenium and tellurium. Recent work by this group has explored the potential fluxional behaviour of normally terdentate ligands which are acting in a bidentate chelate manner. Ligands recently investigated in this context include hybrid S/P/S donors such as bis[*o*-(methylthio)phenyl]phenylphosphine and tris[*o*-(methylthio)-phenyl]phosphine,[1,2] hybrid S/N/S donors such as 2,6-bis-(*p*-tolylthiomethyl)pyridine (L^1) and 2,6-bis(methylthiomethyl)-pyridine (L^2)[3] and N/N/N donors such as 2,2′:6′,2″-terpyridine (terpy).[4–6]

The halogenotricarbonylrhenium(I) complexes of L^1,[3] L^2[3] and terpy[4,6,7] were shown by dynamic NMR spectroscopy to undergo a fluxional process in which the pendant donor group exchanged with the equivalent co-ordinated donor group. Two possible mechanisms were proposed[3,4,6] for the exchange process but it did not prove possible to distinguish between them at that time. However, extensive NMR studies on the halogenotrimethylplatinum(IV) complexes of terpy[4,6] *did* elucidate a mechanism for the fluxional process which, in this case, involves 1,4 shifts of donor N atom pairs.

The question now arises as to whether an analogous mechanism is operative in ligand complexes with unlike donor atoms. To this end we chose to study the analogous $PtXMe_3$ complexes of the ligands L^1 and L^2, where N/S atom pairs are involved.

Experimental

Materials.—The halogenotrimethylplatinum(IV) compounds were prepared by previously published methods.[8,9] The ligands 2,6-bis(*p*-tolylthiomethyl)pyridine[10] and 2,6-bis(methylthiomethyl)pyridine[3,11] were also synthesised by literature methods.

† *Supplementary data available:* see Instructions for Authors, *J. Chem. Soc., Dalton Trans.*, 1993, Issue 1, pp. xxiii–xxviii.

Synthesis of Complexes.—All complexes were prepared *via* the same route. All manipulations were performed under an atmosphere of dry, oxygen free nitrogen in freshly dried[12] and degassed solvents, using standard Schlenk techniques.[13] The procedure for [$PtBrMe_3L^1$] is given below.

[2,6-*Bis*(p-*tolylthiomethyl*)*pyridine*]*bromotrimethyl-platinum*(IV). Bromotrimethylplatinum(IV) (0.4 g, 0.312 mmol) was added to a stirred solution of 2,6-bis(*p*-tolylthiomethyl)-pyridine (0.5 g, 1.42 mmol) in benzene (30 cm^3). After *ca.* 18 h stirring at *ca.* 50 °C, the resultant pale green solution was concentrated to dryness *in vacuo* and the solid washed with light petroleum (b.p. 40–60 °C). Recrystallisation from dichloromethane and hexane afforded 0.32 g (38%) of the white crystalline product. Synthetic and analytical data are given in Table 1.

Physical Methods.—Infrared spectra of the complexes were recorded as CsI discs on a Nicolet Magna FT-IR spectrometer in the region 4000–200 cm^{-1}. Proton NMR spectra were obtained using a Bruker AM250 FT spectrometer, operating at 250.13 MHz. All spectra were recorded as $CDCl_3$ solutions. Chemical shifts are quoted relative to tetramethylsilane as an internal standard. Band shape analyses of the temperature-dependent spectra were performed using the authors' own version of the DNMR3 program.[14] Computer simulated spectra were visually fitted with those experimentally obtained. Two-dimensional exchange (EXSY) spectra were obtained using the NOESYPH[15a] automation program. Peak intensities were obtained by volume integration. Integrations were performed five times and an average value used to calculate the rate constant, using our D2DNMR program.[15b] The NMR probe temperature was controlled by a B-VT variable temperature unit, with the calibration being checked against a Comark digital thermometer. Probe temperatures are considered to be accurate to within ± 1 °C. Activation parameters were calculated from a least-squares fit of the Arrhenius and Eyring plots. The errors quoted in $\Delta G^{\ddagger}$ are those defined by Binsch and Kessler.[16]

Elemental analyses were carried out by Butterworth Laboratories Ltd., Teddington, Middlesex.

Crystal Structure Determination of [$PtBrMe_3L^1$].—*Crystal data*. $C_{24}H_{30}BrNPtS_2$, M = 671.625, monoclinic, space group $P2_1/n$, a = 8.649(2), b = 22.524(3), c = 12.873(3) Å, β = 100.49(1)°, U = 2465.88 Å^3, Z = 4, D_c = 1.809 g cm^{-3}, $F(000)$ = 1304, Mo-Kα radiation (λ = 0.710 69 Å), μ = 175.28 cm^{-1}.

Data collection and processing. Data were obtained using a FAST TV area detector diffractometer situated at the window of a rotating anode generator operating at 50 kV, 55 mA with a molybdenum anode as previously described.[17] The total number of reflections recorded was 12 896, giving 6140 unique [merging R = 0.002 after absorption correction (max., min. transmission factors = 1.330 and 0.886)] and 4628 with $F_o > 3\sigma(F_o)$.

Structural analysis and refinement. The structure was solved by Patterson methods. Full-matrix least-square refinements were performed with non-hydrogen atoms assigned anisotropic thermal parameters. Hydrogen atoms were allowed to float on their parent carbon atoms in the calculated positions (C–H 0.96 Å). Unit weights were applied. For the 284 variables, the final R and R' values were 0.031 and 0.035 respectively. The computer programs used for the structural determination are published elsewhere.[18]

Additional material available from the Cambridge Crystallographic Data Centre comprises H-atom coordinates, thermal parameters and remaining bond lengths and angles.

Results and Discussion

Moderate yields of the complexes [$PtXMe_3L^1$] (X = Cl or Br) were obtained as air-stable, white crystalline solids by the above method. It did not, however, prove possible to prepare the remaining four complexes of this series, *i.e.* [$PtIMe_3L^1$] and [$PtXMe_3L^2$] (X = Cl, Br or I). The reason for this would appear to be their instability in solution. The ambient-temperature ^{1}H NMR spectra (303 K) of the chloro and bromo complexes of L^1 show a single broad platinum methyl resonance indicating that platinum methyl scrambling, a well known feature of complexes of Pt^{IV},[19] is occurring at a significant rate on the one-dimensional NMR time-scale. This rapid equilibration of the platinum methyl environments can only take place if the metal moiety is very loosely bound. Furthermore, both the present complexes showed signs of significant decomposition at temperatures above *ca.* 40–50 °C (see below).

The infrared spectra of the complexes show three bands in the C–H stretching region, characteristic of a *fac* arrangement of the halogenotrimethylplatinum(IV) moiety.[20–22] The presence of three Pt–C stretches and one Pt–N stretch indicates a bidentate chelate structure in which the ligand is co-ordinated to the metal centre *via* the nitrogen of the pyridine ring and one sulfur atom. The bidentate structure is also supported by the elemental analyses. X-Ray crystallography provided confirmation of this conclusion (see below). Infrared, synthetic and analytical data are given in Table 1.

Low-temperature ^{1}H *NMR Studies*.—The ambient-temperature ^{1}H NMR spectra showed broad unresolved resonances. However, on cooling to *ca.* −40 °C the spectral lines sharpened to give well resolved spectra. The results obtained for [$PtBrMe_3L^1$] will serve to illustrate the analysis of the problem. The spectrum at 233 K consists of two principal regions of interest (Fig. 1): (*i*) the platinum and ligand methyl region (*ca.* δ 0.5–2.4) and (*ii*) the ligand methylene region (*ca.* δ 4.4–5.9).

The platinum–methyl region consists of two sets of three resonances (with platinum-195 satellites) of widely differing intensity. The two sets of signals were attributed to the two possible sulfur invertomers, labelled *cis* and *trans* with respect to the orientation of the co-ordinated sulfur *p*-tolyl group to the halogen (Fig. 2). The *cis* isomer is disfavoured on steric grounds (since the halogen has a greater steric bulk than the methyl) and the major invertomer is therefore expected to be the one in which the *p*-tolyl group of the co-ordinated sulfur atom is *cis* to the axial platinum methyl. This is clearly evidenced in the spectrum by the high-field shift of the axial platinum methyl resonance of the major isomer, brought about by the shielding induced by the aromatic ring current. The assignments of the axial and equatorial resonances were based on the *trans* influences of the halogen and the ligand.[23] The ligand methyl signals consist of a strong pair (labelled E,F) due to the *trans* invertomer partially overlapping with a weak pair (labelled O,P) due to the *cis* species.

The ligand methylene region consists of four sets of AB quartets, two of high intensity and two of low intensity. Two of the AB quartets, labelled AB(*trans*) and KL(*cis*), were widely spaced and were attributed to the methylene signals of the chelate ring, since they will be more sensitive to the orientation of the sulfur *p*-tolyl group. The large chemical shift differences reflect the considerable shielding anisotropy of the aromatic ring. The strongly coupled AB quartets due to the methylene in

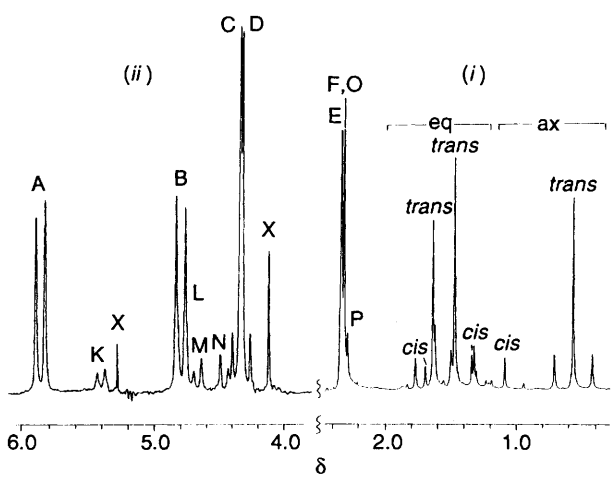

Fig. 1 250 MHz ^{1}H NMR spectrum of [$PtBrMe_3L^1$] at 233 K showing (*i*) the methyl region and (*ii*) the ligand methylene region. Signal labelling of the latter refers to Fig. 2. Impurities denoted by X

Table 1 Synthetic and analytical data for the complexes [$PtXMe_3L^1$] (X = Cl or Br)

Complex	Reaction time (h)	Yield[a] (%)	ν(CH)[b]	ν(PtC)[b]	ν(PtN)[b]	ν(PtX)[b]	Analysis[c] (%) C	H	N
				cm^{-1}					
[$PtClMe_3L^1$]	40	49	2815.2s	567.0w	428.1w	242.1w	43.15	4.50	2.05
			2899.4s	593.0w			(42.95)	(4.50)	(2.10)
			2975.0s	603.0w					
[$PtBrMe_3L^1$]	18	38	2814.7s	562.9w	427.7w	<200	45.90	4.65	2.20
			2899.7s	593.2w			(45.80)	(5.15)	(2.20)
			2973.9s	601.1w					

[a] Yield quoted relative to [$(PtXMe_3)_4$]. [b] Recorded as CsI discs; s = strong, w = weak. [c] Calculated values in parentheses.

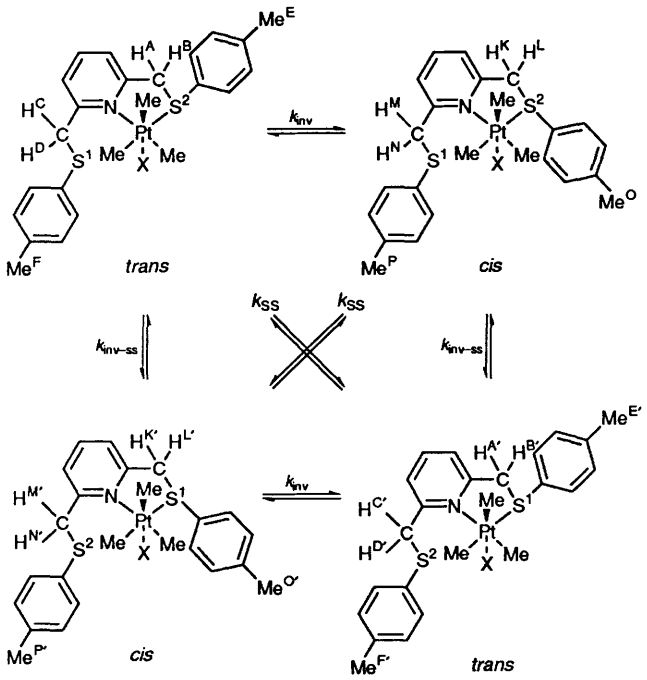

Fig. 2 The *cis* and *trans* isomers of the complexes $[PtXMe_3L^1]$ (X = Cl or Br) showing the interconversion pathways associated with pyramidal S inversion and S–S switching

the unco-ordinated *p*-tolylthiomethyl pyridine are labelled CD(*trans*) and MN(*cis*) in Fig. 1.

The population of the two invertomers, calculated from the relative intensities of both the axial platinum methyl resonances and the AB quartets was found to be 89 (*trans*):11 (*cis*) for the bromo complex and 83:17 for the chloro complex. The slightly higher population of the minor invertomer in the chloro complex reflects the smaller steric bulk of the chloride compared to the bromide.

The ligand aromatic region was not fully resolved due to the small chemical shift differences between the resonances. These signals, therefore, could not be unambiguously assigned. The static NMR parameters for all methyl and methylene protons are given in Table 2.

Variable-temperature ^{1}H *NMR Studies.*—Variable-temperature ^{1}H NMR experiments were carried out on $CDCl_3$ solutions of both complexes. On warming above −40 °C, changes were observed in all regions of the spectrum. In the methylene region, the AB quartets due to the non-equivalent protons of the chelate ring of the *cis* species (protons K and L) (Fig. 1) started to broaden indicating the pyramidal inversion of the co-ordinated sulfur atom interchanging the *cis* and *trans* invertomers. A similar broadening of the AB quartet associated with the pendant methylene protons (protons M and N) (Fig. 1) was also observed. On further warming, the broadening of all four AB quartets increased substantially indicating an exchange between the chelate and pendant methylene protons. Eventually a single broad resonance was observed but it did not prove possible to reach the fast exchange limit of the spectrum due to an intermolecular exchange process with a solution state impurity. The concentration of the impurity appeared to increase with the temperature, suggesting a thermal decomposition product.

Similarly, the platinum methyl region showed broadening indicative of pyramidal sulfur inversion and S–S switching. Platinum methyl axial–equatorial exchange was also observed, leading eventually to a single time-averaged Pt–Me signal.

The methylene AB quartets were submitted to a full band-shape analysis according to the dynamic scheme shown in Fig. 2.

The sulfur inversion and sulfur–sulfur switching processes cause an interconversion between the methylene hydrogens according to dynamic spin system (1).

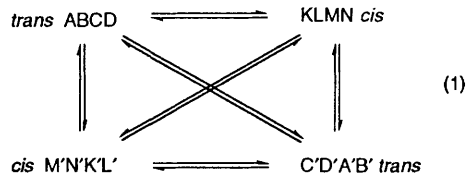

Since there is no scalar coupling between chelate and pendant methylene groups in either invertomer this spin system can be reduced to a degenerate pair of two-spin systems (2).

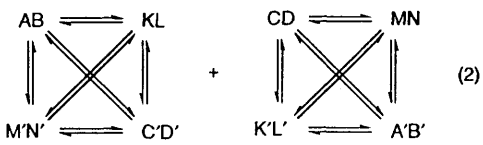

Methylene signal bandshapes were analysed on this basis. It was found necessary to fit the experimental spectra (Fig. 3) to three independent rate constants, namely k_{inv} which defines *trans–cis* exchange without S^1–S^2 exchange, k_{ss} which defines S^1–S^2 exchange within *trans* or *cis* invertomer species, and k_{inv-ss} which defines simultaneous S inversion and S^1–S^2 exchange. Experimental and computer simulated bandshapes for $[PtBrMe_3L^1]$ are shown in Fig. 3, and the 'best fit' rate constants in Table 3. The Arrhenius and Eyring parameters are given in Table 4. It should be noted that it is unlikely that the spectral lineshapes can be fitted to a unique set of 'best-fit' rate constants, and hence the values obtained for the activation parameters must be interpreted with some caution.

It would appear from the magnitude of the energy barriers for all three processes that these internal motions are quite strongly correlated. Indeed, it seems probable that the weakening of the Pt–S bond resulting from the pyramidal inversion of the co-ordinated sulfur atom is quite sufficient to initiate the S–S exchange process.

The activation energies, $\Delta G^{\ddagger}$, for the S^1–S^2 exchange process are in the range 60–63 kJ mol^{-1}, somewhat lower than the magnitudes found for the rhenium analogues $[ReX(CO)_3L^1]$ and $[ReX(CO)_3L^2]$[3] where values are *ca.* 77–78 kJ mol^{-1}. This ordering of $\Delta G^{\ddagger}$ with respect to metal, *i.e.* $Re^{I} > Pt^{IV}$, is consistent with the trends found in the terpyridine[4–6] and sulfur-ligand complexes.[19]

There does not appear to be any obvious halogen trend for any of the three processes. However, with only two complexes being studied and the likely non-uniqueness of spectral bandshape fittings to three independent rate constants it is not possible to draw any firm comparisons.

As with the analogous halogenotricarbonylrhenium(I) complexes[3] two possible mechanisms can be postulated (Fig. 4). Mechanism (*i*) involves a loosening of the Pt–S bond brought about by the pyramidal inversion of the sulfur atom, followed by a 180° rotation about the Pt–N bond. Co-ordination of the 'pendant' sulfur atom reproduces an identical structure. An analogous mechanism to this was assumed to occur in the $[M\{PPh(o\text{-}MeSC_6H_4)_2\}X_2]$ complexes[2] (M = Pt^{II} or Pd^{II}, X = Cl or Br). However, in that case a rotation of only *ca.* 109° (the tetrahedral angle) was necessary to bring the pendant SMe group close enough to form a five-co-ordinate transient state during the S–S switching. The much larger angle of rotation involved in the present complexes and the considerable steric interaction between the halogen and one of the thioaryl groups makes such a mechanism less favourable. The second mech-

Table 2 Proton NMR chemical shift data[a] in $CDCl_3$ for the complexes $[PtXMe_3L^1]$ (X = Cl or Br) at 233 K

Complex	Invertomer population (%)	δ(Pt–Me)[b,c]	δ(CH_2)[b,c]	Label	SC_6H_4Me
$[PtClMe_3L^1]$	83.1 (*trans*)	0.55 (73.41) (a)	4.32 (15.24) (p)	D	2.33
		1.44 (74.40) (e)	4.74 (16.72) (c)	C	2.31
		1.53 (66.16) (e)	4.39 (15.24) (p)	B	
			5.78 (16.72) (c)	A	
	16.9 (*cis*)	0.59 (72.91) (a)	4.66 (15.72) (p)	N	2.34
		1.08 (73.41) (e)	4.47 (15.72) (p)	M	2.28
		1.61 (68.45) (e)	4.83 (13.74) (c)	L	
			5.51 (13.74) (c)	K	
$[PtBrMe_3L^1]$	89.0 (*trans*)	0.56 (72.91) (a)	4.34 (12.50) (p)	D	2.33
		1.47 (74.39) (e)	4.42 (12.50) (p)	C	2.31
		1.64 (68.40) (e)	4.85 (13.92) (c)	B	
			5.87 (13.92) (c)	A	
	11.0 (*cis*)	1.09 (71.50) (a)	4.50 (10.00) (p)	N	2.31
		1.34 (75.80) (e)	4.72 (10.00) (p)	M	2.29
		1.69 (69.00) (e)	4.80 (12.60) (c)	L	
			5.39 (12.60) (c)	K	

[a] Chemical shifts quoted relative to tetramethylsilane as an internal standard. [b] a = axial, e = equatorial, p = pendant, c = chelated. [c] $^2J_{PtH}$/Hz and $^2J_{HH}$/Hz in parentheses.

Table 3 'Best fit' first-order rate constants (s^{-1}) for fluxional processes in $[PtBrMe_3L^1]$

T/K	k_{inv}	k_{SS}	k_{inv-SS}
248	0.5	≈0	≈0
253	1.0	0.8	≈0
258	2.0	1.3	≈0
263	5.0	2.9	2.0
273	15.0	7.0	12.0
278	25.0	12.0	20.0
283	55.0	20.0	40.0
288	85.0	28.0	75.0
293	120	38.0	135
303	200	75.0	240

anism [mechanism (*ii*) Fig. 4] involves a simultaneous loosening of both the Pt–S and Pt–N bonds and an associated twist about the X–Pt–CH_3 axis equal to the N–Pt–S(1) angle [θ = 81.5° (see later)], giving a seven-co-ordinate transition state. This mechanism has recently been shown to occur in the halogenotrimethylplatinum(IV) complexes of terpyridine[6] where the ligand was acting as an N/N bidentate chelate. However, in the complexes being studied here, two different types of bond need to be loosened simultaneously, namely a Pt–S bond and a possibly stronger Pt–N bond, which might favour the rotation mechanism (*i*). The mechanism actually occurring will therefore depend on two competing factors, namely, the steric interaction of the *p*-tolylthiomethyl group with the $PtXMe_3$ moiety concomitant with a 180° rotation about the Pt–N bond, and the relative strengths of the Pt–N and Pt–S bonds.

The two fluxional mechanisms are theoretically distinguishable in the halogenotricarbonylrhenium(I) complexes by their effect on the equatorial carbonyl environments of the $ReX(CO)_3$ moiety. Unfortunately, this effect proved impossible to measure because the low solubility of the complexes prevented variable-temperature ^{13}C NMR measurement of their carbonyl signals.[3] However, in the present platinum(IV) complexes, the mechanism should be deducible by ^1H NMR spectroscopy since mechanism (*i*) (Fig. 4) does not lead to an equivalencing of the equatorial platinum methyl resonances, whereas mechanism (*ii*) (Fig. 4) does. Unfortunately the Pt–Me region is very crowded (Fig. 1) due to the presence of both *trans* and *cis* invertomers. One-dimensional variable-temperature studies are further complicated by the fact that, at elevated temperatures where the S–S exchange fluxion proceeds at a measurable rate, exchange of all three Pt–Me environments (Pt–Me scrambling) also occurs. Two-dimensional EXSY experiments were therefore preferred since these would provide kinetic information on the effects of S inversion and S–S switching at temperatures low enough effectively to freeze out any Pt–Me scrambling. Hydrogen-1 two-dimensional EXSY spectra were accordingly recorded at five temperatures in the range 243–263 K, and cross-peaks between the two distinct equatorial Pt–Me signals of the major *trans* species (labelled Me^1 and Me^2 in Fig. 4) were detected. The absence of cross-peaks between the axial (Me^3) and equatorial Pt–Me confirmed the absence of Pt–Me scrambling at these temperatures. The two-dimensional EXSY spectrum of $[PtBrMe_3L^1]$ at −10 °C is shown in Fig. 5. In this spectrum weak cross-peaks are also observed between *trans* and *cis* axial and between *trans* and *cis* equatorial Pt–Me signals due to S inversion without S–S switching. The activation energy for the S–S exchange fluxion agreed well with the one-dimensional bandshape analysis-based value (see Table 4) thereby supporting the accuracy of both one- and two-dimensional methods and providing unambiguous evidence for the 'tick-tock' twist mechanism (*ii*) of fluxion in these complexes. Implicit in this mechanism is a close comparability in energy of the two bonds which must loosen simultaneously in this process. In order to provide further insight into the relative lengths/strengths of the Pt–N and Pt–S bonds in these complexes a crystal structure of the bromide complex was obtained.

Crystal Structure of $[PtBrMe_3L^1]$.—A view of the molecule indicating the atomic numbering scheme is shown in Fig. 6. This clearly shows the expected *fac* octahedral geometry and the bidentate chelate nature of the ligand. The fractional atomic coordinates for the crystal structure are given in Table 5. Selected bond distances and angles are given in Table 6. It should be noted that the Pt–N bond length [2.311(6) Å] is significantly shorter than the Pt–S bond [2.419(4) Å]. This will be due primarily to the different atomic radii of N and S, since the two platinum–ligand bonds must be of comparable strengths for both to be involved in the fluxional rearrangement.

Inspection of the bond angles reveals a small deviation from an idealised octahedral geometry [N–Pt–S(1) 81.5°], resulting from the steric requirements of the ligand. This deviation is however about 5° smaller than that observed for $[PtIMe_3(terpy)]$[5] indicating that 2,2′:6′,2″-terpyridine has a smaller bite size than 2,6-bis(*p*-tolylthiomethyl)pyridine.

The crystal structure reveals the *trans* sulfur invertomer to be

Table 4 Arrhenius and Eyring parameters[a] for the complexes $[PtXMe_3L^1]$ (X = Cl or Br)

Complex	Fluxional process	E_a/kJ mol^{-1}	$\log_{10}(A/s^{-1})$	$\Delta S^{\ddagger}$/J K^{-1} mol^{-1}	$\Delta H^{\ddagger}$/kJ mol^{-1}	$\Delta G^{\ddagger}$/kJ mol^{-1}
$[PtClMe_3L^1]$	Inversion	61.3 (3.95)	12.95 (0.75)	−4.6 (14.3)	59.0 (3.9)	60.38 (0.32)
	S–S switch	*c*	*c*	*c*	*c*	59.98 (0.29)
	Inversion/S–S	*c*	*c*	*c*	*c*	65.72 (0.22)
$[PtBrMe_3L^1]$	Inversion	71.5 (2.5)	14.82 (0.48)	31.1 (9.3)	69.2 (2.5)	59.94 (0.24)
	S–S switch	59.9 (1.5)	12.29 (0.29)	−17.3 (5.7)	57.6 (1.5)	62.78 (0.15)
	S–S switch[d]	68.2 (4.7)	13.90 (0.96)	14.2 (18.3)	66.1 (4.6)	61.89 (0.83)
	Inversion/S–S	80.4 (4.5)	16.39 (0.91)	61.1(17.6)	78.1 (4.7)	59.86 (0.28)

[a] Errors given in parentheses. [b] $\Delta G^{\ddagger}$ values quoted at 298 K. [c] Restricted temperature range gave unreliable values. [d] Calculated from two-dimensional EXSY experiments.

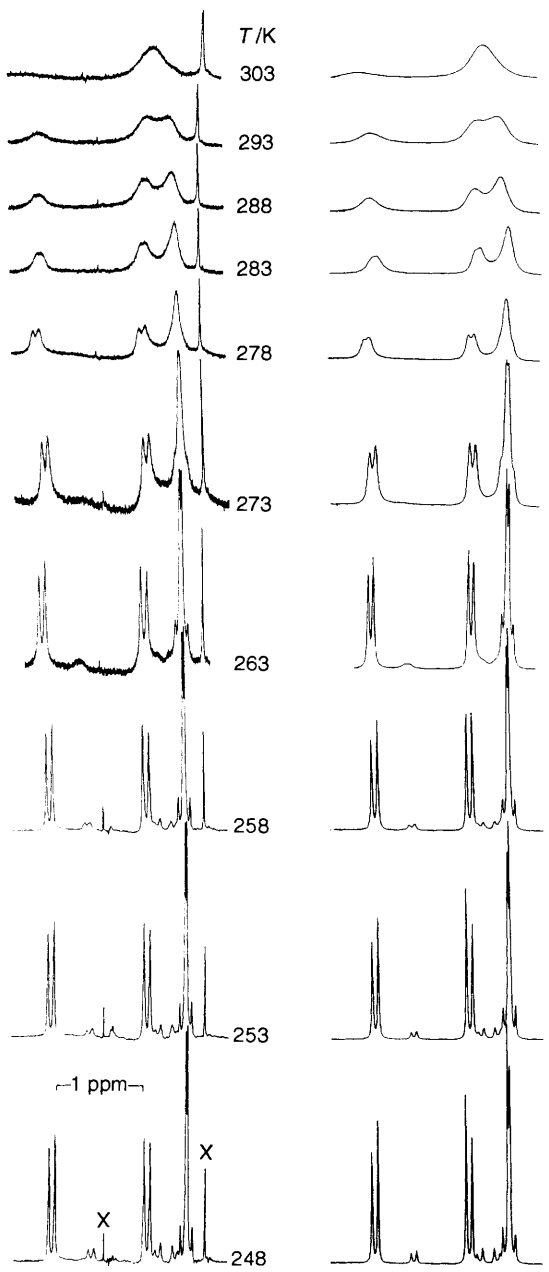

Fig. 3 Variable-temperature ^1H NMR spectra of $[PtBrMe_3L^1]$ in the range 233–303 K showing the effects of S inversion and S–S switching fluxions. Computer simulated spectra shown alongside are based on the rate constants in Table 3. The signal X is decomposition product

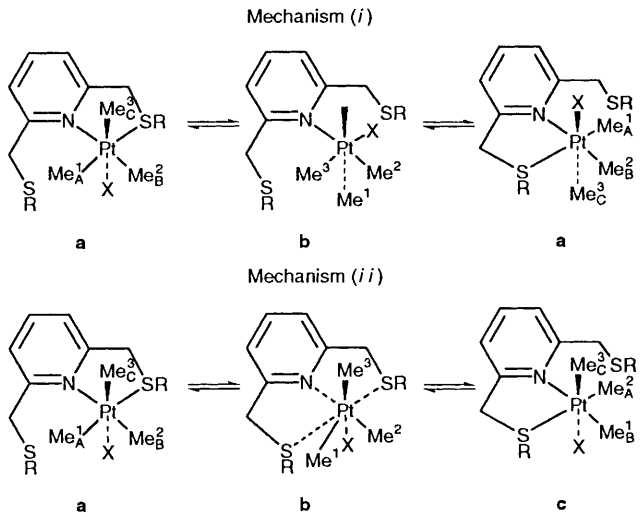

Fig. 4 The two possible mechanisms for the S–S exchange fluxion

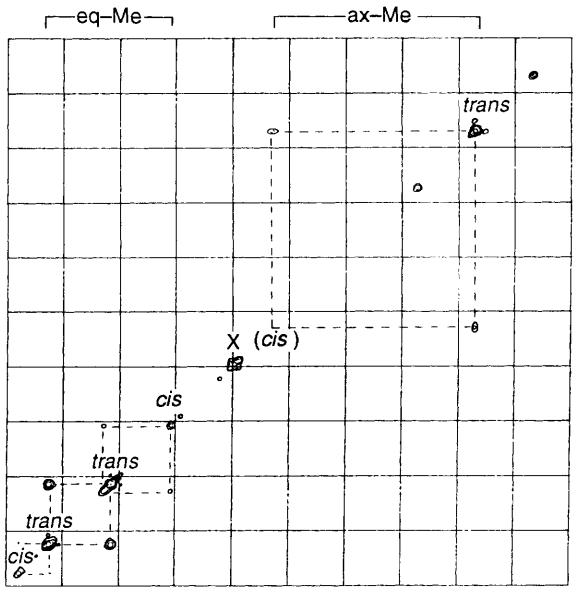

Fig. 5 The ^1H two-dimensional EXSY NMR spectrum of $[PtBrMe_3L^1]$ at 263 K showing the exchange of the two *trans* equatorial Pt–Me environments resulting from the S–S exchange. Cross-peaks are observed between the main signals and between their low frequency ^{195}Pt satellites. The additional weak cross-peaks are due to *cis–trans* exchange without S–S switching. Note that the diagonal signal of the *cis*-axial PtMe group [denoted by (*cis*)] is not detected at this contour level of the two-dimensional spectral map. The signal X is probably water

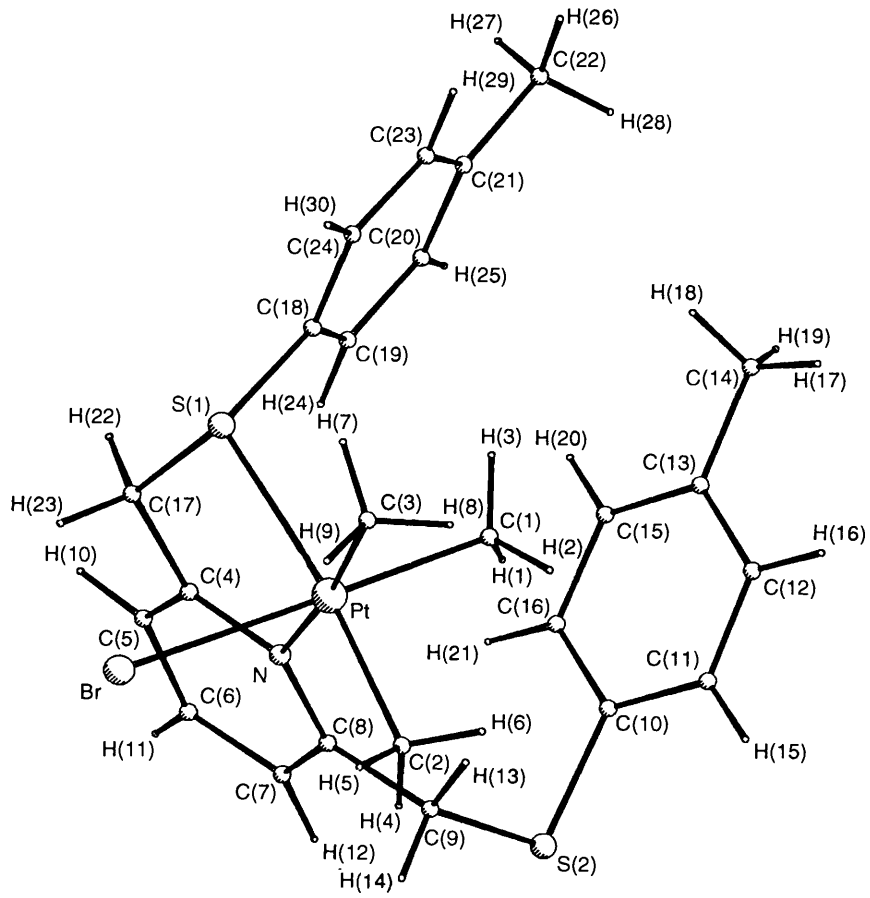

Fig. 6 A view of the crystal structure of [$PtBrMe_3L^1$] showing the atom labelling

Table 5 Fractional atomic coordinates (× 10^4) for *fac*-[$PtBrMe_3L^1$]

Atom	*x*	*y*	*z*
Pt	3730.8(3)	5713.5(1)	2502.2(2)
Br	4454.3(8)	4655.6(3)	1901.2(5)
S(1)	2774(2)	5201(1)	3910(1)
S(2)	−107(2)	6943(1)	−203(1)
C(1)	3195(9)	6545(3)	2973(5)
C(2)	4755(8)	6060(3)	1303(5)
C(3)	5912(8)	5830(4)	3438(6)
N	1171(5)	5557(2)	1653(3)
C(4)	387(7)	5134(3)	2111(5)
C(5)	−1140(7)	4963(3)	1677(5)
C(6)	−1870(7)	5208(3)	752(5)
C(7)	−1097(7)	5647(3)	293(5)
C(8)	389(7)	5822(3)	766(4)
C(9)	1174(7)	6324(3)	284(5)
C(10)	−258(8)	7269(3)	1035(5)
C(11)	697(9)	7737(3)	1408(6)
C(12)	710(10)	7961(3)	2404(7)
C(13)	−254(9)	7722(3)	3049(6)
C(14)	−234(15)	7974(5)	4127(8)
C(15)	−1235(10)	7277(3)	2654(6)
C(16)	−1264(8)	7037(3)	1665(6)
C(17)	1187(8)	4817(3)	3077(5)
C(18)	1839(7)	5678(3)	4694(5)
C(19)	340(7)	5903(3)	4403(5)
C(20)	−222(8)	6295(4)	5087(6)
C(21)	668(8)	6476(3)	6045(5)
C(22)	16(11)	6885(5)	6765(7)
C(23)	2172(8)	6236(3)	6310(5)
C(24)	2752(8)	5842(3)	5663(5)

Table 6 Selected bond lengths (Å) and angles (°) for *fac*-[$PtBrMe_3L^1$]

Br–Pt	2.616(4)	S(1)–Pt	2.419(4)
C(1)–Pt	2.048(9)	C(2)–Pt	2.067(8)
C(3)–Pt	2.062(8)	N–Pt	2.311(6)
C(17)–S(1)	1.802(8)	C(18)–S(1)	1.768(9)
C(9)–S(2)	1.819(8)	C(10)–S(2)	1.781(9)
C(4)–N	1.363(8)	C(8)–N	1.356(8)
C(5)–C(4)	1.391(9)	C(17)–C(4)	1.491(10)
C(6)–C(5)	1.360(10)	C(7)–C(6)	1.383(11)
C(8)–C(7)	1.376(9)	C(9)–C(8)	1.509(10)
S(1)–Pt–Br	85.4(1)	C(1)–Pt–Br	179.2(2)
C(1)–Pt–S(1)	95.1(3)	C(2)–Pt–Br	88.0(3)
C(2)–Pt–S(1)	172.4(2)	C(2)–Pt–C(1)	91.5(4)
C(3)–Pt–Br	92.7(4)	C(3)–Pt–S(1)	91.4(3)
C(3)–Pt–C(1)	86.7(4)	C(3)–Pt–C(2)	85.3(4)
N–Pt–Br	88.9(2)	N–Pt–S(1)	81.5(2)
N–Pt–C(1)	91.8(3)	N–Pt–C(2)	102.0(3)
N–Pt–C(3)	172.6(3)	C(17)–S(1)–Pt	96.3(3)
C(18)–S(1)–Pt	113.0(3)	C(18)–S(1)–C(17)	104.7(4)
C(10)–S(2)–C(9)	98.5(4)	C(4)–N–Pt	114.3(4)
C(8)–N–Pt	128.3(5)	C(8)–N–C(4)	117.4(6)
C(5)–C(4)–N	122.1(6)	C(17)–C(4)–N	120.2(6)
C(17)–C(4)–C(5)	117.6(6)	C(6)–C(5)–C(4)	119.6(7)
C(7)–C(6)–C(5)	118.7(7)	C(8)–C(7)–C(6)	120.0(7)
C(7)–C(8)–N	122.0(7)	C(9)–C(8)–N	118.9(6)
C(9)–C(8)–C(7)	119.1(6)	C(8)–C(9)–S(2)	115.1(5)
C(11)–C(10)–S(2)	119.6(7)	C(16)–C(10)–S(2)	121.3(6)
C(4)–C(17)–S(1)	117.0(5)	C(19)–C(18)–S(1)	125.0(6)
C(24)–C(18)–S(1)	115.3(6)	C(24)–C(18)–C(19)	119.7(7)

present in the solid state, supporting the assignment of the *trans* invertomer as the major solution-state isomer.

Conclusion

This work has shown that the recently discovered 1,4-metallotropic shift observed in bidentate nitrogen chelates is

not restricted to complexes of like donor atoms (*e.g.* N/N) but may occur in complexes with unlike donors (*e.g.* N/S), providing the bond energies are not too dissimilar. The mechanism in all cases is a 'tick-tock' twist of the metal moiety through the ligand bite angle. In the present complexes with L^1 this process is strongly correlated with pyramidal inversion of the co-ordinated sulfur atom and scrambling of the Pt–Me environments.

Acknowledgements

We thank the University of Exeter for a scholarship (to P. J. H.) and Dr. Vladimir Šik for helpful advice on the two-dimensional EXSY methodology.

References

1 E. W. Abel, D. Ellis, K. G. Orrell and V. Šik, *Polyhedron*, 1991, **10**, 1603.
2 E. W. Abel, J. C. Dormer, D. Ellis, K. G. Orrell, V. Šik, M. B. Hursthouse and M. A. Mazid, *J. Chem. Soc., Dalton Trans.*, 1992, 1073.
3 E. W. Abel, D. Ellis and K. G. Orrell, *J. Chem. Soc., Dalton Trans.*, 1992, 2243.
4 E. W. Abel, N. J. Long, K. G. Orrell, A. G. Osborne, H. M. Pain and V. Šik, *J. Chem. Soc., Chem. Commun.*, 1992, 303.
5 E. W. Abel, V. S. Dimitrov, N. J. Long, K. G. Orrell, A. G. Osborne, V. Šik, M. B. Hursthouse and M. A. Mazid, *J. Chem. Soc., Dalton Trans.*, 1993, 291.
6 E. W. Abel, V. S. Dimitrov, N. J. Long, K. G. Orrell, A. G. Osborne, H. M. Pain, V. Šik, M. B. Hursthouse and M. A. Mazid, *J. Chem. Soc., Dalton Trans.*, 1993, 597.
7 E. R. Civetello, P. S. Dragovich, T. B. Karpishin, S. G. Novick, G. Bierach, J. S. O'Connell and T. D. Westmoreland, *Inorg. Chem.*, 1993, **32**, 237.
8 J. C. Baldwin and W. C. Kaska, *Inorg. Chem.*, 1975, **14**, 2020.
9 D. H. Goldsworthy, Ph.D. Thesis, University of Exeter, 1980.
10 D. Parker, J. M. Lehn and J. Rimmer, *J. Chem. Soc., Dalton Trans.*, 1985, 1517.
11 D. Ellis, Ph.D. Thesis, University of Exeter, 1989.
12 D. D. Perrin and W. L. F. Armarego, *Purification of Laboratory Chemicals*, Pergamon, Oxford, 1988.
13 D. F. Shriver, *Manipulation of Air-sensitive Compounds*, McGraw-Hill, New York, 1969.
14 D. A. Kleier and G. Binsch, Program DNMR3, Quantum Chemistry Program Exchange, Indiana University, IN, 1970.
15 (*a*) G. Bodenhausen, H. Kogler and R. R. Ernst, *J. Magn. Reson.*, 1984, **58**, 370; (*b*) E. W. Abel, T. P. J. Coston, K. G. Orrell, V. Šik and D. Stephenson, *J. Magn. Reson.*, 1986, **70**, 34.
16 G. Binsch and H. Kessler, *Angew. Chem., Int. Ed. Engl.*, 1980, **19**, 411.
17 A. A. Danopoulos, M. B. Hursthouse, B. Hussain-Bates and G. Wilkinson, *J. Chem. Soc., Dalton Trans.*, 1991, 1855.
18 SHELX 76, G. M. Sheldrick, Program for Crystal Structure Determination and Refinement, University of Cambridge, 1976; DIFABS, N. P. C. Walker and D. Stuart, *Acta Crystallogr., Sect. A*, 1983, **39**, 158.
19 E. W. Abel, S. K. Bhargava and K. G. Orrell, *Prog. Inorg. Chem.*, 1984, **32**, 1.
20 D. E. Clegg, J. R. Hall and G. A. Swile, *J. Organomet. Chem.*, 1972, **38**, 403.
21 J. R. Hall, *Essays in Structural Chemistry*, eds. A. J. Downs, D. A. Long and L. A. K. Staveley, Macmillan, London, 1974, p. 433.
22 A. Psaila, Ph.D. Thesis, University of Exeter, 1977.
23 T. G. Appleton, H. C. Clark and L. E. Manzer, *Coord. Chem. Rev.*, 1973, **10**, 335.

Received 28*th June* 1993; *Paper* 3/03650B